

Distribution of exchange energy in a bond-alternating $S = 1$ quantum spin chainA. Zheludev,¹ T. Masuda,¹ B. Sales,¹ D. Mandrus,¹ T. Papenbrock,^{2,3} T. Barnes,^{2,3} and S. Park^{4,5}¹Condensed Matter Sciences Division, Oak Ridge National Laboratory, Oak Ridge, TN 37831-6393, USA.²Department of Physics and Astronomy, University of Tennessee, Knoxville, TN 37996-1200, USA.³Physics Division, Oak Ridge National Laboratory, Oak Ridge, TN 37831-6373, USA.⁴NIST Center for Neutron Research, National Institute of Standards and Technology, Gaithersburg, MD 20899, USA.⁵Department of Materials Science and Engineering,
University of Maryland, College Park, MD 20742, USA.

(Dated: March 22, 2024)

The quasi-one-dimensional bond-alternating $S = 1$ quantum antiferromagnet $\text{Ni}(\text{N}^0\text{-bis}(3\text{-aminopropyl})\text{propane-1,3-diamine})(\text{NO}_2)\text{ClO}_4$ (NTENP) is studied by single crystal inelastic neutron scattering. Parameters of the measured dispersion relation for magnetic excitations are compared to existing numerical results and used to determine the magnitude of bond-strength alternation. The measured neutron scattering intensities are also analyzed using the 1st-moment sum rules for the magnetic dynamic structure factor, to directly determine the modulation of ground state exchange energies. These independently determined modulation parameters characterize the level of spin dimerization in NTENP. First-principle DMRG calculations are used to study the relation between these two quantities.

PACS numbers: 75.10.Pq, 75.40.Gb, 75.40.Mg, 75.30.Ds

I. INTRODUCTION

Integral antiferromagnetic (AF) spin chains are best known for having an exotic spin liquid ground state with a characteristic gap in the magnetic excitation spectrum.^{1,2} The Haldane gap has been subject to intensive theoretical and experimental studies for the last two decades, and is by now very well characterized and understood. The spin wave function of the Haldane ground state is not known exactly, but is similar to the easy to visualize Valence Bond Solid (VBS) state.³ The latter is constructed by representing each $S = 1$ spin as two separate $S = 1/2$ spins, binding pairs of these into antiferromagnetic dimers for each exchange bond, and projecting the resulting state back onto the subspace where $S_i^2 = 2$ on each site. This wave function is the exact ground state of the Aleck-Kennedy-Lieb-Tasaki (AKLT) model,⁴ and is schematically shown in the left inset of Fig. 1. Each exchange link carries exactly one valence bond, and the periodicity of the underlying crystal lattice remains intact. Considerably less attention has been given to a different quantum spin liquid ground state that is realized in integral spin chains with alternating exchange interactions. As the alternation parameter $\delta = (J_1 - J_2)/(J_1 + J_2)$ deviates from zero (uniform chain), the energy gap decreases and closes at some critical value $\delta_c = 0.26$,^{5,6,7,8,9,10,11} as illustrated in Fig. 1. Further increasing δ beyond this quantum-critical point re-opens the spin gap. The ground state is then no longer the Haldane state, but, instead, a dimerized one. The corresponding valence bond wave function is shown in right inset in Fig. 1. It contains two valence bonds on each strong link and none at all on the weaker ones.

The two gapped quantum phases differ by their "hidden" symmetries.^{9,12} The Haldane state is characterized

by a non-vanishing expectation value for the antiferromagnetic string order parameter,¹³ related to a breaking of a non-local $Z_2 \times Z_2$ symmetry.¹² This order parameter vanishes in the dimerized phase, where $Z_2 \times Z_2$ remains completely intact.^{9,12} The highly non-local multi-spin correlation function that defines antiferromagnetic strings can not be expressed through the usual pair spin correlation functions $\langle S_i^{(\alpha)}(0) S_j^{(\alpha)}(t) \rangle$. As a result, the "hidden" string order can not be directly observed in scattering or other type of experiments. In fact, one does not expect any qualitative differences in observable spin correlation functions of alternating $S = 1$ chains with similar gap energies on different sides of the phase diagram. Distinguishing the two phases in a real $S = 1$ alternating-chain compound is therefore a challenging task, involving a careful quantitative analysis of the data.

A model alternating $S = 1$ -chain material suitable for experimental studies was discovered only recently.¹⁴ This compound is $\text{Ni}(\text{N}^0\text{-bis}(3\text{-aminopropyl})\text{propane-1,3-diamine})(\text{NO}_2)\text{ClO}_4$, NTENP for short, is structurally similar to well-known Haldane-gap systems NENP¹⁵ and NDMAP.^{16,17} Unlike the latter, NTENP features a distinctive alternation of short and long bonds in the antiferromagnetic $S = 1$ Ni^{2+} chains.¹⁸ Extensive bulk measurements on NTENP were performed by Narum et al. and are reported in Ref. 14. Susceptibility data^{14,18} shows that in NTENP $\delta \approx 0.4$, almost the same as in a Haldane spin chain.¹⁹ Anisotropy effects aside, on the simplified phase diagram of an alternating $S = 1$ chain⁷ shown in Fig. 1 NTENP must be located somewhere on the dashed horizontal line. This line crosses the theoretical curve for $\delta(\delta_c)$ twice: at $\delta < \delta_c$ (near the Haldane point $\delta_c = 0$) and at $0.40 > \delta_c$. Bulk measurements can not directly probe the microscopic alternation parameter δ . Nevertheless, Hagiwara et al. were able to conclude that NTENP is in the dimerized phase based on indirect ev-

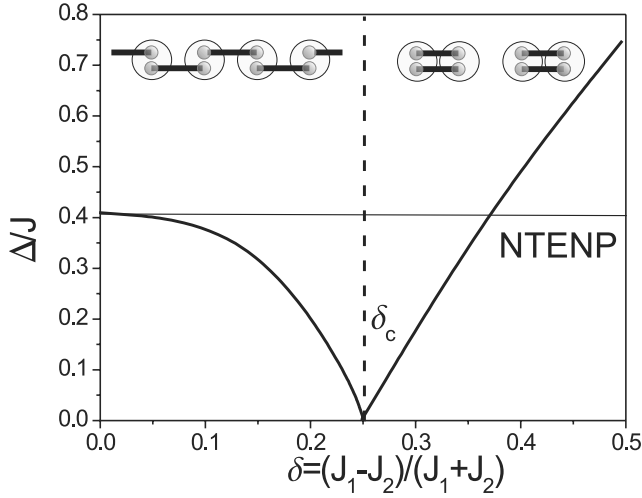


FIG. 1: Field dependence of energy gap in a bond-alternating $S = 1$ quantum antiferromagnet, based on numerical results by S. Yamamoto, Ref. 7. A quantum critical point (dashed line) separates the Haldane phase, similar to the VBS state (left inset) from the dimerized state (right inset). The possible location of NTEP is indicated by the thin horizontal line.

idence, namely the behavior of non-magnetic impurities in this material.¹⁴ The main purpose of the present work is to use a microscopic probe (inelastic neutron scattering) to directly measure exchange alternation and other crucial parameters of undoped NTEP. Our experimental findings are discussed in comparison with first-principles DMRG calculations.

II. EXPERIMENTAL APPROACH

Before describing the actual neutron scattering experiments performed as part of this study, we shall discuss the measurement strategies. In particular, we need to identify those measurable physical quantities that are most sensitive to the effect of bond alternation.

A. Structural consideration

The triclinic crystal structure of NTEP is visualized in Fig. 2.^{14,20} The $S = 1$ chains are composed of Ni^{2+} ions octahedrally coordinated in an organic environment. The chains run along the a axis, one chain per unit cell. While all Ni^{2+} sites are crystallographically equivalent, the Ni-Ni distances within the chains alternate between $d_1 = 4.28 \text{ \AA}$ and $d_2 = 4.36 \text{ \AA}$. Intra-chain Ni-Ni links are covalent and pass through structurally disordered NO_2 groups. Inter-chain interactions are of Van der Waals nature and therefore much weaker. The crystallographic symmetry is low, space group $P\bar{1}$. The lattice constants at room temperature are $a = 10.75 \text{ \AA}$, $b = 9.41 \text{ \AA}$,

$$c = 8.79 \text{ \AA}, \quad \alpha = 95.52^\circ, \quad \beta = 108.98^\circ, \quad \text{and} \quad \gamma = 106.83^\circ.^{18}$$

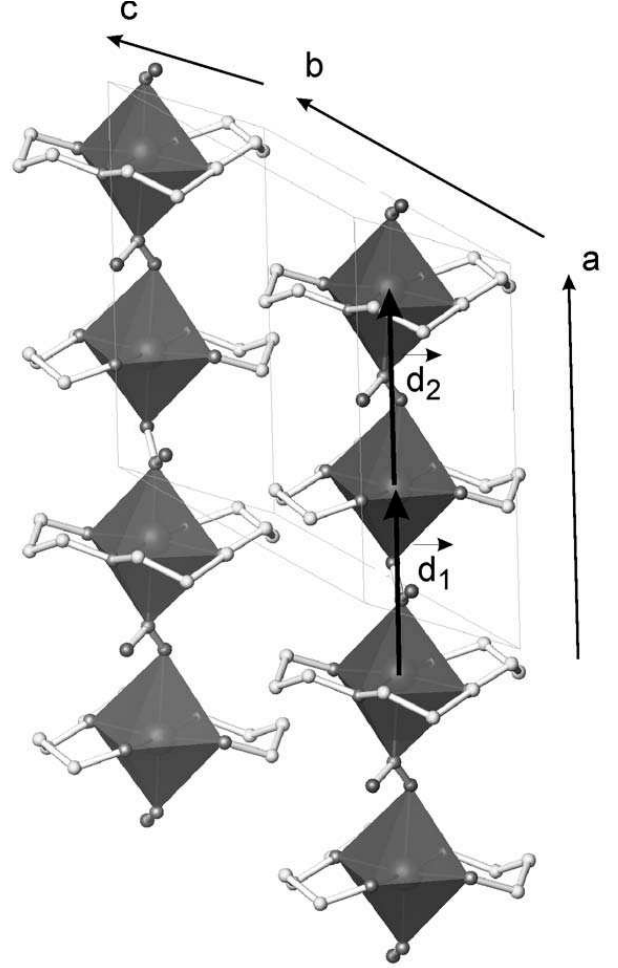


FIG. 2: A schematic view of the bond-alternating $S = 1 \text{ Ni}^{2+}$ chains in the triclinic crystal structure of NTEP. The equatorial vertices of the Ni^{2+} coordination octahedra are nitrogen atoms. The octahedra are coupled via chemically disordered NO_2 groups. Oxygen and nitrogen atoms are shown as dark grey spheres. Light grey spheres are carbon atoms. Hydrogen atoms and intercalated CD_4 solvent molecules are not shown. The alternation of short and long bonds in the chains is characterized by bond vectors d_1 and d_2 , respectively.

In the following discussion we will use the following coordinate system: x is chosen along the a axis, z is along c , and y completes a right-handed set of axes.

B. Model Hamiltonian and observable energy scales

A model Hamiltonian for NTEP was proposed in Ref. 14. In the present work we shall employ a slightly different, but equivalent form:¹⁹

$$\hat{H} = J \sum_j (1 - \hat{S}_{2j} \hat{S}_{2j+1}) + J \sum_j (1 + \hat{S}_{2j} \hat{S}_{2j-1}) + D \sum_j (\hat{S}_j^{(x)})^2 \quad (1)$$

Inter-chain spin interactions are expected to be very weak and are not included in the above expression. The exchange constant J is, itself, not directly observable experimentally. However, it can be reliably inferred from an analysis of the measured temperature dependence of bulk susceptibility: for NTENP $J = 3.4$ meV.^{14,18}

A directly measurable quantity related to J is zone-boundary energy $h!_{zb}$, defined as the minimum energy of magnetic excitations with momentum transfer $q_{zb} = \frac{\pi}{a}$, where a is the distance between next-nearest-neighbor spins. In NTENP a is simply the lattice constant. For a uniform (Haldane) chain with $\beta = 0$ numerical simulations show that $h!_{zb} = 2.7J$.^{21,22,23,24} It is easy to verify that $h!_{zb} = 2J$ for isolated dimers ($\beta = 1$). The complete β -dependence of $h!_{zb}$ was recently determined in a systematic numerical study.²⁵ It is important to note that unlike $\beta = J$, $h!_{zb} = J$ is a monotonic function of β , and can be used to unambiguously determine whether a particular material is in the dimerized or Haldane phases.

Another directly observable energy scale is spin wave velocity v . Numerically, $v = 2.49J$ for a uniform chain²³ and $v = 0$ for the other limiting case of isolated $S = 1$ dimers. The gap energies for different spin polarizations are also experimentally accessible. For an isotropic uniform chain $\Delta = 0.41J$.^{21,22,23,24} For isolated dimers with $\beta = 1$, $\Delta = 2J$. According to a simple perturbation theory argument,^{26,27} the polarization-averaged energy gap $\Delta = \frac{1}{3}\Delta$ is, to a good approximation, the same as in the isotropic system with $D = 0$. The gap for excitations polarized along the x , y and z axes can then be written as:

$$\begin{aligned} \Delta_x &= \bar{\Delta} + 2\bar{D}; \\ \Delta_z &= \bar{\Delta} - \bar{D}; \end{aligned} \quad (2)$$

The observable splitting \bar{D} is proportional to the microscopic anisotropy parameter D in the Hamiltonian. Numerical simulations indicate that for a uniform chain $\bar{D} = \frac{2}{3}D$.^{27,28} For isolated dimers one simply has $\bar{D} = D$. For NTENP the gap energies can be estimated from high-field magnetization measurements of Naim et al.¹⁴ The critical field at which the gap for one of the spin polarizations is driven to zero by the Zeeman effect is given by $g_B H_c^{(x)} = \frac{P}{\beta}$.^{28,29,30} For NTENP $H_c^{(x)} = 9.3$ T, $H_c^{(y)} = H_c^{(x)} = 12.4$ T, and $g = 2.14$. This gives $\Delta_z = 1.15$ meV and $\Delta_x = 2.06$ meV. From this one gets $\bar{\Delta} = 1.45$ meV ($\beta = J = 0.43$) and $\bar{D} = 0.3$ meV ($D = J = 0.1$).⁴⁶

The important energy scales $\bar{\Delta}$, $h!_{zb}$, v and \bar{D} can be straightforwardly measured in inelastic neutron scattering experiments, by mapping out the dispersion relation

of magnetic excitations. They do not, however, carry any direct information on the level of dimerization in the system.

C. Exploiting the 1st-moment sum rule

Additional insight can be drawn from an analysis of neutron scattering intensities of magnetic excitations. In fact, these intensities directly relate to the strengths of individual magnetic bonds. One way of extracting this information is by making use of the Hohenberg-Brinkman 1st-moment sum rule for the magnetic dynamic structure factor.^{31,32} This method has been previously successfully applied to the analysis of inelastic neutron scattering data on several occasions: for recent examples see Refs. 33,34. For the Hamiltonian (1) the sum rule, an exact expression, can be written as:³²

$$\begin{aligned} \sum_{\mathbf{q}} (h!) S(\mathbf{q};!) d(h!) &= \frac{1}{2N} h \hat{S}_{\mathbf{q}}^{(x)}; \hat{S}_{\mathbf{q}}^{(x)}; \hat{H} \quad i = \\ &= \sum_{\mathbf{q}} 2J_1 \sin^2(qd_1=2) (1 - \hat{S}_{2j}^{(x)} \hat{S}_{2j+1}^{(x)}) i \\ &= \sum_{\mathbf{q}} 2J_2 \sin^2(qd_2=2) (1 - \hat{S}_{2j}^{(x)} \hat{S}_{2j-1}^{(x)}) i \\ &= 2D (1 - \sum_x (\hat{S}_j^{(x)})^2) i + h \hat{S}_j^{(x)}; \hat{S}_j^{(x)}; \hat{S} (S+1) : (3) \end{aligned}$$

Here d_1 and d_2 are real-space vectors chosen along the short and long bonds in the chains, respectively, and \hat{S} label the coordinate axes: x , y and z . In practice it may be quite difficult to separately measure all three diagonal components of \hat{S} . Fortunately, for NTENP the ratio $D = J$ is only about 10% (see discussion above), and, to a good approximation, the correlators $h \hat{S}_{2j}^{(x)} \hat{S}_{2j+1}^{(x)} i$ and $h \hat{S}_{2j}^{(x)} \hat{S}_{2j-1}^{(x)} i$ are independent of the subscript. The last term in Eq. 3 scales as $(D = J)^2$ (Ref. 26) and can be entirely neglected in our case. Under these assumptions the sum rule becomes:

$$\begin{aligned} \sum_{\mathbf{q}} (h!) S(\mathbf{q};!) d(h!) &= \\ &= \frac{4}{3} E_1 \sin^2(qd_1=2) - \frac{4}{3} E_2 \sin^2(qd_2=2): \end{aligned} \quad (4)$$

The quantities $E_1 = J_1 h \hat{S}_{2j} \hat{S}_{2j+1} i$ and $E_2 = J_2 h \hat{S}_{2j} \hat{S}_{2j-1} i$ are ground state exchange energies associated with the strong and weak bonds, respectively. Due to the translational invariance, they do not depend on the site index j .

Eq. 4 directly relates the intensities measured in an inelastic neutron scattering experiment to the modulation of exchange energy in the spin chains

$$\tilde{\sim} = \frac{E_1 - E_2}{E_1 + E_2}; \quad (5)$$

While certainly not equivalent to $\tilde{\sim}$, $\tilde{\sim}$ is a very natural measure of the magnitude of "dimerization" of the ground state. In the isotropic (Heisenberg) case of $D = 0$ it can be directly expressed through $\tilde{\sim}$ and the ground state energy $E(\tilde{\sim})$ as:

$$\begin{aligned} \tilde{\sim} &= \frac{D}{X} \sum_j (1 + \tilde{\sim}) S_{2j} S_{2j+1} - \frac{X}{j} \sum_j (1 - \tilde{\sim}) S_{2j-1} S_{2j} = E(\tilde{\sim}) \\ &= -\frac{D}{4} + (1 - \tilde{\sim}^2) \frac{D}{4} \ln E(\tilde{\sim}); \end{aligned} \quad (6)$$

For practical applications Eq. 4 can be further simplified if one assume the single mode approximation (SMA).³⁵

$$S(\mathbf{q}; \omega) = S(\mathbf{q}) \delta(\omega - \omega_{\mathbf{q}}); \quad (7)$$

The sum rule for a bond-alternating chain is then written as:

$$S(\mathbf{q}) = \frac{4}{3|\mathbf{q}|} [E_1 \sin^2(\mathbf{q} \cdot \mathbf{d}_1 = 2) + E_2 \sin^2(\mathbf{q} \cdot \mathbf{d}_2 = 2)]; \quad (8)$$

For isolated dimers expression 7 is exact. For a uniform spin chain the SMA works remarkably well in most of the Brillouin zone, especially in the vicinity of the 1D AF zone-center where the Haldane gap is observed.^{34,36,37} Near the quantum critical point, where $\tilde{\sim}$ vanishes, the SMA will fail entirely. However, for NTENP $\tilde{\sim} = J$ is similar to that in a uniform chain, and the SMA should still be reliable near the 1D zone-center \mathbf{q}_0 , $\mathbf{q}_0 \cdot (\mathbf{d}_1 + \mathbf{d}_2) = 2$. In this range the SMA dispersion relation can be written in the standard "relativistic" form:

$$(\hbar \omega_{\mathbf{q}})^2 = \tilde{\sim}^2 + v^2 \sin^2(\mathbf{q} \cdot \mathbf{a}) \quad (9)$$

D. Application to NTENP

The main experimental difficulty in using Eq. 8 to estimate the ratio $\tilde{\sim}$ in NTENP is the fact that the bond vectors $\mathbf{d}_1 = 0.521\mathbf{a} + 0.0246\mathbf{b} - 0.0424\mathbf{c}$ and $\mathbf{d}_2 = 0.479\mathbf{a} - 0.0246\mathbf{b} + 0.0424\mathbf{c}$ are quite close in this material. Fig. 3 shows a grayscale and contour plot of the effective "contrast" ratio

$$C(\mathbf{q}) = \frac{\sin^2(\mathbf{q} \cdot \mathbf{d}_1 = 2) - \sin^2(\mathbf{q} \cdot \mathbf{d}_2 = 2)}{\sin^2(\mathbf{q} \cdot \mathbf{d}_1 = 2) + \sin^2(\mathbf{q} \cdot \mathbf{d}_2 = 2)} \quad (10)$$

as a function of momentum transfer in the $(h; 0; l)$ reciprocal-space plane in NTENP. This ratio is a good measure of our sensitivity to $\tilde{\sim}$. Immediately one can see

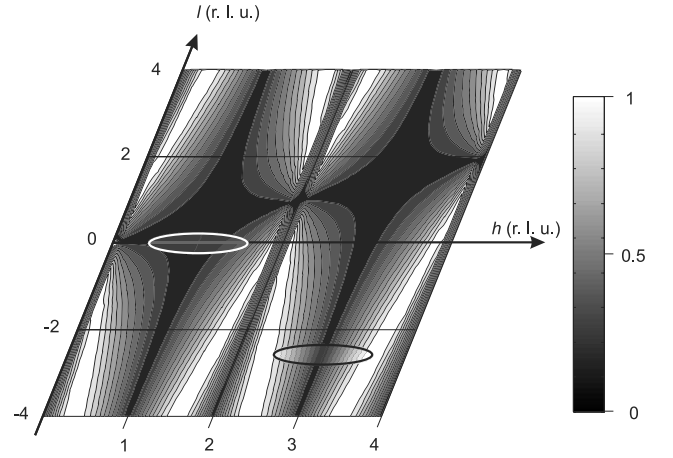


FIG. 3: Contrast ratio $C(\mathbf{q})$ (Eq. 10) for distinguishing ground state exchange energies based on inelastic neutron intensities as a function of momentum transfer in the $(h; 0; l)$ reciprocal-space plane of NTENP. The circled areas are regions of reciprocal space where most of the inelastic data were measured.

that E_1 and E_2 can not be distinguished based on the data collected at the 1D AF zone-centers, where $C(\mathbf{q})$ vanishes. This is rather unfortunate, since it is at these wave vectors that the dispersion $\omega_{\mathbf{q}}$ is a minimum, and excitation intensity is maximized due to the $1/\omega_{\mathbf{q}}$ factor in Eq. 8. A high contrast is achieved away from the 1D AF zone-centers, and at large momentum transfers. However, under these conditions the magnetic scattering is weakened by the $1/\omega_{\mathbf{q}}$ coefficient and the effect of ionic magnetic form factors. Away from the AF zone-centers the applicability of the SMA also becomes questionable. Finally, the phonon background becomes progressively important at large $|\mathbf{q}|$ and interferes with the measurements. In our experiments we have found that a reasonable compromise between intensity, contrast and noise level can be achieved on either side of the $h = 3$ 1D zone-center. Most of the data described in Section IV C below were collected in that region of reciprocal space, represented in Fig. 3 by the circled area in the lower-right.

III. EXPERIMENTAL PROCEDURES

Translucent dark-purple plate-like single crystal samples of 50% deuterated NTENP were grown in aqueous solution. Four such crystals were co-aligned in one "super-sample" with a total mass of 1.5 g and mosaic spread of 2.5° . Inelastic neutron scattering experiments were performed at two different facilities. Lower-energy excitations (up to 3 meV energy transfer) were investigated using the SPINS cold-neutron 3-axis spectrometer installed at the NIST Center for Neutron Research. Neutrons with a fixed final energy $E_f = 3.7$ meV were utilized with a BeO filter after the sample. A Pyrolytic Graphite PG (002) monochromator was used in com-

bination with a θ at (Setup I) or horizontally focusing (Setup II) PG analyzers. Additional beam collimation was provided by the neutron guide and (open) 80° 80° (open) collimators (Setup II employed a radial post-sample collimator). Thermal-neutron studies were performed using the HB-1 3-axis spectrometer installed at the High Flux Isotope Reactor, Oak Ridge National Laboratory. The data were collected with $E_i = 13.5$ meV xed-incident energy neutrons (Setup III). PG (002) reflections were employed in both monochromator and analyzer. A PG filter was installed in front of the sample to eliminate higher-order beam contamination. Beam collimation was 48° 40° 40° 240° .

The sample being only partially deuterated led to a substantial geometry-dependent attenuation of the neutron beam due to incoherent scattering from hydrogen nuclei. This effect is equivalent to neutron absorption, and can be fully compensated for using the technique described in Ref. 38. For every inelastic scan measured, one performs a separate elastic scan to determine the effective neutron transmission corrections. For every point of the "transmission" scan the sample rotation and scattering angles are set exactly as in the inelastic scan. Unless a Bragg condition is accidentally satisfied in the sample, the main contribution to scattering in the "transmission" scan is due to incoherent elastic processes in the sample. To a good approximation, the corresponding cross section is isotropic and independent of neutron energy. The intensity detected in the "transmission" scan is therefore directly proportional to the neutron transmission in the sample. Normalizing the original inelastic scan by the measured transmission correction not only gets rid of absorption effects, but also compensates for the any geometric corrections that occur when a large asymmetric sample rotates in a finite-size neutron beam in the course of the scan. In various scans measured in the present work the effective transmission coefficient varied by roughly a factor of 2 in the course of each scan or between different scans.

IV. EXPERIMENTAL RESULTS

A. Gap energies: constant- q data

The gap energies and anisotropy splitting of the excitation triplet were accurately measured using cold-neutron Setups I and II. Energy scans collected at 1D AF zone-centers $(1;0;0)$ (Fig. 4a) and $(3;0;0)$ (Fig. 4b) with Setup I show a single sharp peak at about 1.2 meV energy transfer. The background for these scans was measured, point-by-point at $q = (1.5;0;0)$ and $(2.5;0;0)$, respectively. As shown, the scans are corrected for transmission effects. The data in Fig. 4 were collected with the scattering vector q directed perpendicular to the $(b;c)$ crystallographic plane, and therefore represent fluctuations of y and z spin components of the triplet. The resolution of the present experiment is insufficient to unambiguously

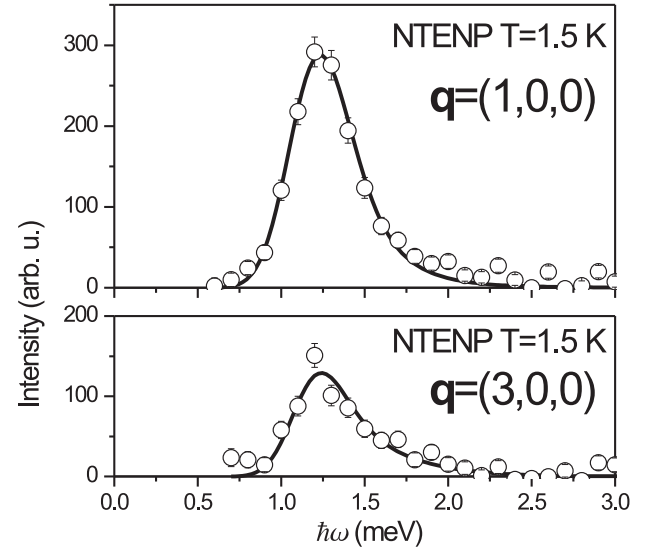


FIG. 4: Inelastic scans collected at the $(1;0;0)$ and $(3;0;0)$ 1D antiferromagnetic zone-centers in NTENP (symbols). The data were taken using a cold neutron 3-axis spectrometer with a θ analyzer. The solid lines are fits to the data as described in the text.

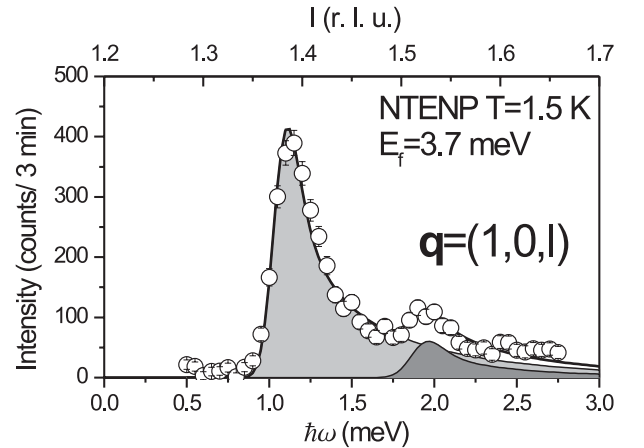


FIG. 5: Inelastic scan at the $q = (1;0;1)$ 1D antiferromagnetic zone-center measured using a horizontally-focusing analyzer. The heavy solid line is a fit to the data as described in the text. The light-grey and dark-grey shaded areas represent partial contributions of gap excitations polarized parallel and perpendicular to the crystallographic $(b;c)$ plane, respectively.

resolve the gaps for y - and z -polarized modes. To detect the x -axis spin fluctuations we performed additional measurements with a large momentum transfer perpendicular to the chains. In the focusing-analyzer mode (Setup II) the scattering vector was at all times maintained on the $(1;0;1)$ reciprocal-space rod. For each energy transfer, the transverse momentum transfer l was chosen to have the sample chain axis parallel to the scattered neutron

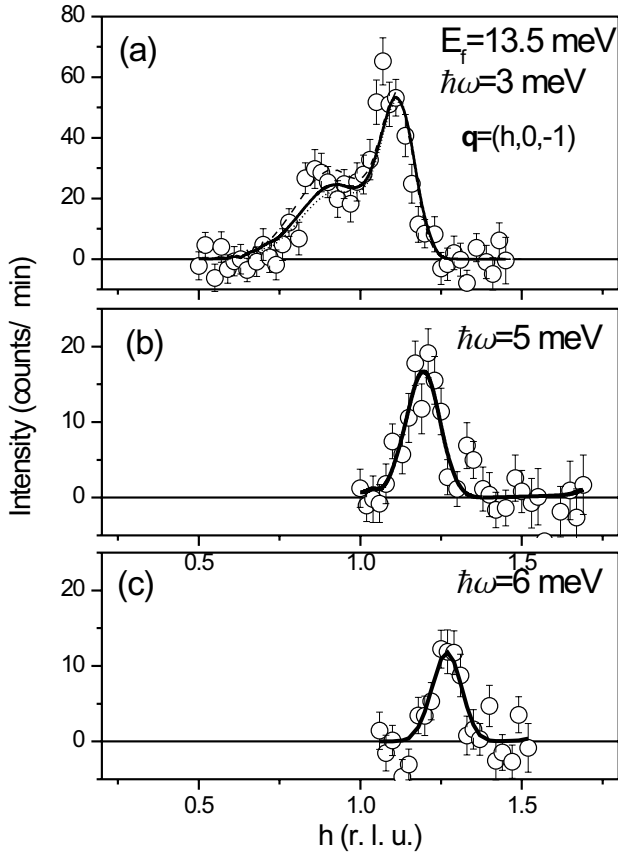


FIG. 6: Constant-E scans measured in NTENP in the vicinity of the $(1;0;0)$ AF zone-center (symbols). The dashed and dotted lines in (a) are profiles simulated assuming a cross section function as given by Eqs. 8 & 9 with $\tilde{\omega} = 1$ and $\tilde{\omega} = 1$, respectively. The solid line in (a) is a global fit to several scans, as described in the text. The solid lines in (b) and (c) are fits to single scans.

beam. This geometry optimizes q -resolution along the chains. The resulting scan is shown in Fig. 5. Due to the intrinsic polarization-dependence of the magnetic scattering cross-section, the largest contribution to this scan is from y and x -polarized excitations. The new feature observed at about 1.8 meV energy transfer was thus attributed to x -axis spin fluctuations. Note that the lower-energy peak in Fig. 5 appears at a slightly lower energy than in the scan taken with the scattering vector parallel to the chain axis. This behavior is likely due to a weak dispersion of excitations perpendicular to the chains.

The constant- Q scans were analyzed assuming a simple single-mode cross section as given by Eqs. 7, 8 and 9. The spin wave velocity was fixed at $v = 8.6$ meV, as separately determined from the analysis of constant-E scans described below. The usual polarization factors for unpolarized neutrons determined the relative intensities of the in-plane and out-of-plane spin fluctuations. In addition, a magnetic form factor for Ni^{2+} was explicitly included in the cross section function. The re-

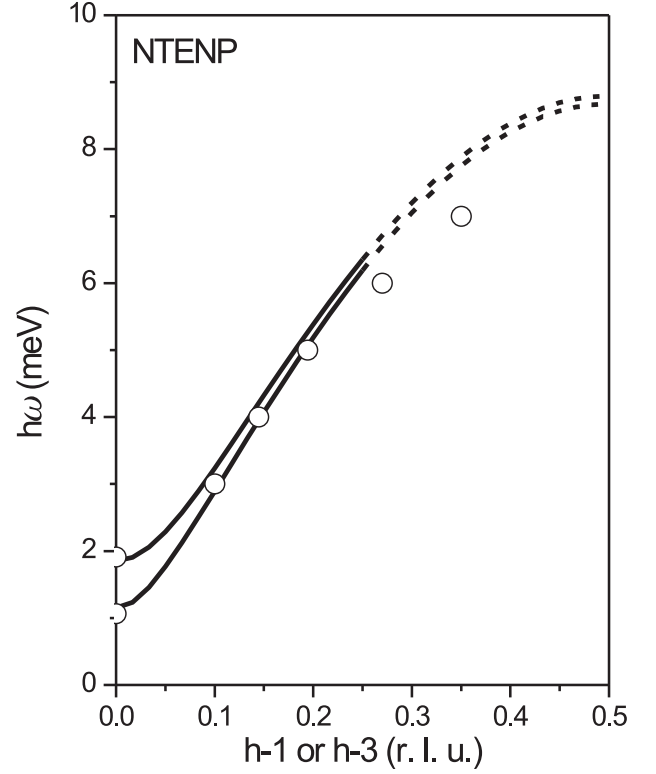


FIG. 7: Measured dispersion relation of magnetic excitations in NTENP (symbols). Lines are the result of a global fit of a model cross section to the neutron data as described in the text.

sulting model for the dynamic structure factor was numerically convoluted with the spectrometer resolution function, calculated in the Cooper-Nathans approximation. The only adjustable parameters of the model were the gap energies ω_x , ω_y and ω_z and an overall intensity scaling factor. A very good fit to the scans with zero transverse momentum transfer was obtained with $\omega_y = \omega_z = 1.16(0.01)$, as is shown in solid lines in Fig. 4. Slightly smaller energies of the doublet were obtained by analyzing the data shown in Fig. 5. Here the gap energies were found to be $\omega_y = \omega_z = 1.07(0.01)$ and $\omega_x = 1.91(0.02)$ meV. These values correspond to $\bar{\omega} = 1.35(2)$ meV and $\Delta = 0.28(2)$ meV, in good agreement with bulk measurements of Nanniet al.¹⁴

B. Dispersion relation: constant-E data

The dispersion relation for single-mode excitations in NTENP was measured in constant-E scans. In order to optimize magnetic intensities (form factor) these data were collected around the $(1;0;0)$ AF zone-center (left circled area in Fig. 3). Typical scans are plotted in open symbols in Fig. 6. To take into account resolution effects, but to avoid constraining the dispersion relation to the postulated sinusoidal form, each scan was sepa-

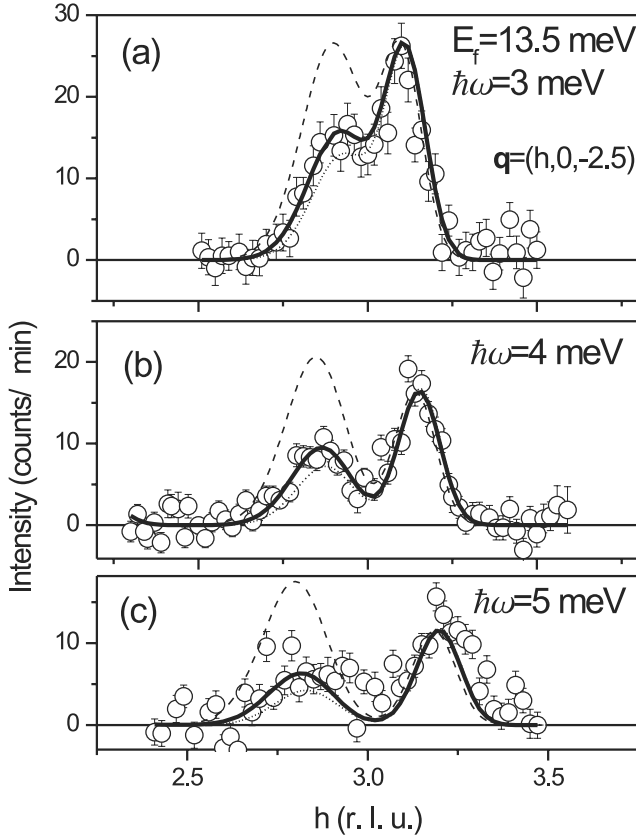


FIG. 8: Constant-E scans measured in NTENP using a thermal-neutron setup in the vicinity of the $(3;0; 2.5)$ AF zone-center (symbols). All lines are as in Fig. 6(a).

rately analyzed using the model cross section described above. The adjustable parameters for each scan were an intensity prefactor and the spin wave velocity v . The gap energies were fixed at the values determined using cold neutrons (see above). Typical fits are shown in Fig. 6(b) and (c) in solid lines. The dispersion relation deduced from such fits to individual scans is plotted in open symbols in Fig. 7.

C. Exchange energy modulation and global fits

All scans described above are fairly insensitive to the distribution of exchange energies in the chains, due to a small contrast ratio at the particular wave vectors. To illustrate this, in Fig. 6(a) we have plotted peak profiles simulated using Eqs. 8(9, and assuming $E_1 = 0$ (dashed line) or $E_2 = 0$ (dotted line). To within the accuracy of our measurements, the two profiles are almost identical. A much better contrast (although a significantly smaller intensity) was achieved in constant-E scans collected along the $(h;0; 2.5)$ reciprocal-space rods around $h = 3$ (right circled area in Fig. 3). These data are plotted in symbols in Fig. 8. A similar constant-E scan was measured using cold neutrons and Setup I, and is plotted

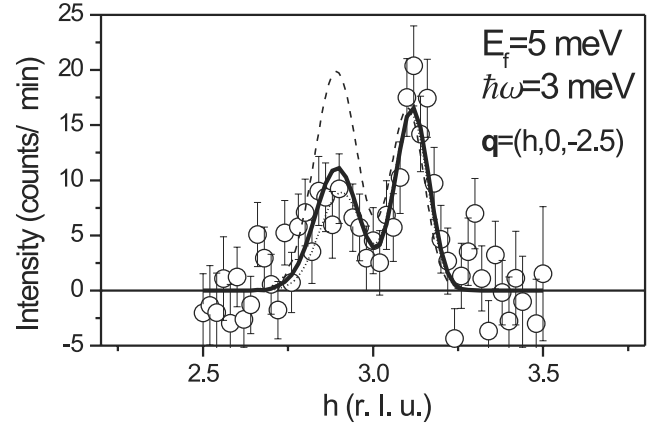


FIG. 9: Constant-E scan measured in NTENP using a cold-neutron setup in the vicinity of the $(3;0; 2.5)$ AF zone-center (symbols). All lines are as in Fig. 6(a).

if Fig. 9. In both figures the dashed and dotted lines are simulations for $E_2 = 0$ or $E_1 = 0$, respectively, assuming $v = 8.6$ meV. From these data the strong dimerization in NTENP becomes apparent: the ground state exchange energy is primarily concentrated on the shorter bonds.

To quantify this observation we performed a global fit to the data collected in constant-E scans measured for energy transfers up to 5 meV with setups I and III. The adjustable parameters were two intensity scaling factors (one for each setup), the spin wave velocity v and the bond-alternation parameter $\tilde{\alpha}$. Very good fits are obtained with $v = 8.6(1)$ meV and $\tilde{\alpha} = 0.42(+0.2; -0.1)$. The large asymmetric error bar on $\tilde{\alpha}$ is unavoidable due to the technical difficulties associated with low intensity, small contrast ratio and transmission corrections.

The simple sinusoidal dispersion curves postulated in Eq. 9 is plotted in lines in Fig. 7 using the experimentally determined gap energies and spin wave velocity. At higher energies the experimental data points clearly lie below these curves. While it is difficult to extrapolate the experimental result to the zone-boundary, one can roughly estimate h_{ZB} to be smaller than v by about 1 meV.

All physical parameters obtained for NTENP in our neutron scattering studies are summarized in Table I in comparison with those obtained by Narumi et al. using bulk techniques¹⁴ and to known exact results for uniform and fully dimerized isotropic $S = 1$ chains.

V. NUMERICAL CALCULATIONS

In order to relate the measured exchange energy modulation parameter $\tilde{\alpha}$ to the alternation of exchange constants J , we performed a numerical study of the model Hamiltonian (1), assuming a vanishing anisotropy $D = 0$. The ground state energy $E(\tilde{\alpha})$ was computed as a function of $\tilde{\alpha}$ using the density matrix renormalization group

TABLE I: Physical parameters for the alternating $S = 1$ chains in NTENP in comparison with those for uniform and fully dimerized isotropic $S = 1$ spin chains.

	NTENP ^a	NTENP ^b	Uniform chain	Isolated dimers
J	3.4 meV	{	{	{
\overline{J}	1.45 meV 0.42J	1.35 (2) meV 0.40 (1)J	0.41J	2J
D	0.3 meV 0.1J	0.28 (2) meV 0.083 (6)J	$\frac{2}{3}D$ ^{27,28}	D
v	{	8.6 (1) meV 2.5 (1)J	2.5J ²³	0
$h!_{ZB}$	{	7.5 (5) meV = 2.2 (1)J	2.7J ²³	2J
$\sim \frac{E_1 - E_2}{E_1 + E_2}$	{	0.42	0	1
$\frac{J_1 - J_2}{J_1 + J_2}$	0.40 or 0 ^c	0.37 (1) or 0.06 (2) ^d 0.30 (0.05) ^e 0.24 (-0.04, + 0.08) ^f	0	1

^aBulk measurements: Ref. 14,18

^bNeutron scattering: this work, assuming $J = 3.4$ meV.

^cFrom $\overline{J} = J$ with \overline{J} deduced from high-field magnetization data and numerical results of Ref. 7.

^dFrom $\overline{J} = J$ with directly measured \overline{J} and numerical results of Ref. 7.

^eFrom $h!_{ZB} = J$ with directly measured $h!_{ZB}$ and numerical results of Ref. 25

^fFrom directly measured \sim and numerical results of this work.

(DMRG) method^{39,40,41} for a chain of 32 spins with periodic boundary conditions. The parameter \sim was then obtained using Eq. 6. These results are plotted in Fig. 10. The computed curve is monotonic and quite smooth in the studied domain of parameter space. Crossing the quantum-critical point at $\delta_c \approx 0.26$ is marked only by a weak point-of-infection-type anomaly. We recall that at δ_c the correlation length diverges. However, for our particular calculation, this does not appear to be a problem. The observable (6) is very smooth and is not subject to significant finite-size corrections. It was verified that doubling of the system size changed the results shown in Fig. 10 by less than one percent.

To justify the use of the isotropic model for computing \sim as a function of δ , we also studied the behavior of the expectation value of the anisotropy term in the Hamiltonian 1. It was found that its contribution to the ground state energy is practically independent of δ and is equal to about $2=3D$ per spin.

V I. D I S C U S S I O N

Our neutron results present new opportunities to determine the magnitude of bond-alternation in NTENP and to place this material on the phase diagram. First of all, \overline{J} can be estimated from the gap energies. Using the numerical results of Ref. 7 and assuming $J = 3.4$ meV¹⁴, for $\overline{J} = 1.35 (2)$ meV one gets $\delta = 0.37 (1)$, assuming NTENP is on the dimerized side of the phase diagram. The alternative is $\delta = 0.06 (2)$ in the Haldane phase, and the distinction can not be made based on gap measure-

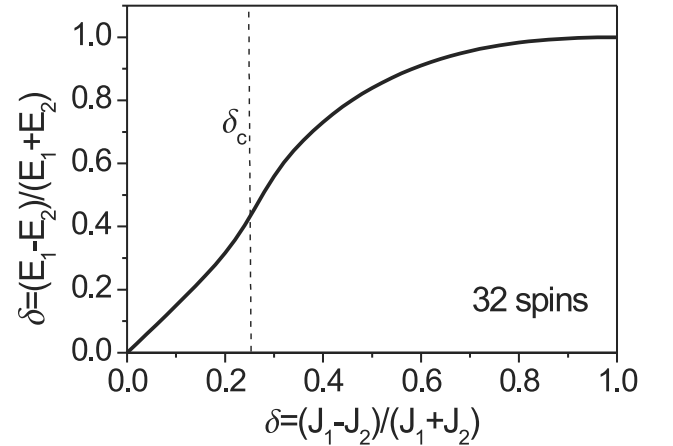


FIG. 10: Alternation of exchange energies $\sim = (E_1 - E_2)/(E_1 + E_2)$ as a function of the alternation of exchange constants δ , computed for a 32-site bond-alternating $S = 1$ chain with periodic boundary conditions. The quantum phase transition at δ_c corresponds to an infection point on the calculated curve.

ments alone.

The numerical results of the previous section allow us to independently estimate based the measured exchange energy alternation. The experimental value $\sim = 0.42 (+0.2; -0.1)$ corresponds to $\delta \approx 0.24 (-0.04; +0.08)$. This value is within 1.5% of the estimate based on the measured gap energy, with the assumption that NTENP is in the dimerized phase. Assuming that NTENP was in the Haldane phase with $\delta = 0.06$ would imply $\sim \approx 0.05$, in

- ²⁷ O. Golinelli, T. Jolicoeur, and R. Lacaze, *J. Phys. Condens. Matter* **5**, 1399 (1993).
- ²⁸ O. Golinelli, T. Jolicoeur, and R. Lacaze, *Phys. Rev. B* **45**, 9798 (1992).
- ²⁹ A. M. Tsvelik, *Phys. Rev. B* **42**, 10499 (1990).
- ³⁰ O. Golinelli, T. Jolicoeur, and R. Lacaze, *J. Phys. Condens. Matter* **5**, 7847 (1993).
- ³¹ P. C. Hohenberg and W. F. Brinkman, *Phys. Rev. B* **10**, 128 (74).
- ³² I. Zaliznyak, Sum rules for the spin dynamic structure factor, unpublished (2000).
- ³³ G. Xu, C. Broholm, D. H. Reich, and M. A. Adams, *Phys. Rev. Lett.* **84**, 4465 (2000).
- ³⁴ I. A. Zaliznyak, S.-H. Lee, and S.-V. Petrov, *Phys. Rev. Lett.* **87**, 017201 (2001).
- ³⁵ See, for example, A. Auerbach, *Interacting Electrons and Quantum Magnetism*, Springer, New York, 1994, chapter 9.
- ³⁶ S. Ma, C. Broholm, D. H. Reich, B. J. Stemli, and R. W. Erwin, *Phys. Rev. Lett.* **69**, 3571 (1992).
- ³⁷ G. Xu, J. F. DiTusa, T. Ito, H. Takagi, C. L. Broholm, and G. Aeppli, *Phys. Rev. B* **54**, R6827 (1996).
- ³⁸ A. Zheludev, S. Maslov, T. Yokoo, J. Akimitsu, S. Raymond, S. E. Nagler, and K. Hirota, *Phys. Rev. B* **61**, 11601 (2000).
- ³⁹ S. R. White, *Phys. Rev. Lett.* **69**, 2863 (1992).
- ⁴⁰ S. R. White, *Phys. Rev. B* **48**, 10345 (1993).
- ⁴¹ For a review see, e.g., I. Peschel, X. Wang, M. Kaulke, and K. Hallberg (Eds.), *Density-Matrix Renormalization Group*, Springer-Verlag, Berlin, 1999.
- ⁴² K. k. M. Hagiwara and I. A. A. eck, *Phys. Rev. Lett.* **65**, 3181 (1990).
- ⁴³ S. H. Glanum, S. Geschwind, K. M. Lee, M. L. Kaplan, and J. Michel, *Phys. Rev. Lett.* **67**, 1641 (1991).
- ⁴⁴ P. P. Mitra, B. I. Halperin, and I. A. A. eck, *Phys. Rev. B* **45**, 5299 (1992).
- ⁴⁵ E. Lieb and D. Mattis, *J. Math. Phys.* **3**, 749 (1962).
- ⁴⁶ Note the discrepancy with Ref. 14, where the authors seemingly fail to distinguish between D and D' . In any case, their quoted estimate ($D=J=0.35$ using the symmetric definition of J) is hard to reconcile with the very small anisotropy of critical field and gap energies that the authors report and that our neutron scattering experiments confirm. We believe that the discrepancy is due to inconsistent notations or a trivial mistake in Ref. 14.